

Ultra Long Single Crystalline $\text{Na}_{0.3}\text{V}_2\text{O}_5$ Nanofibers/Nanorings Synthesized by a Facile One Pot Green Approach and their Lithium Storage Behavior

Ganganagappa Nagaraju

Center for Nano and Material Sciences, Jain Global Campus, Jain University, Jakkasandra Post, Kanakapura Talluk, Bangalore 562 112, India

Neste trabalho, o desenvolvimento de um método hidrotérmico simples para a síntese de nanofibras/nanoanéis de $\text{Na}_{0.3}\text{V}_2\text{O}_5$ em etapa única e sem qualquer surfactante, a 200 °C em 3-5 dias, é relatado. Os produtos foram caracterizados por difratometria de raios X (XRD), espectroscopia no infravermelho com transformada de Fourier (FTIR), espectroscopia UV-Vis, microscopia eletrônica de varredura (SEM), microscopia eletrônica de transmissão (TEM) e teste de descarga-carga eletroquímica para baterias de íon de lítio. Os difratogramas de raios X mostraram que, a 200 °C por 2 e 3-4 dias, formaram-se fitas de $\text{Na}_{0.3}\text{V}_2\text{O}_5 \cdot 1.5\text{H}_2\text{O}$ e nanofibras/anéis de $\text{Na}_{0.3}\text{V}_2\text{O}_5$, respectivamente. O espectro FTIR revelou picos em 1003 e 956 cm^{-1} atribuídos a $\text{V}^{5+}=\text{O}$ e $\text{V}^{4+}=\text{O}$, respectivamente. O espectro UV-Vis mostrou absorvância máxima em 404 nm (3,07 eV). As análises por TEM revelaram uma grande quantidade de fibras com 70-100 nm de espessura e várias dezenas de micrômetros de comprimento. Os anéis apresentaram diâmetro de ca. 20 μm e espessura de 70-150 nm. As nanofibras/anéis exibiram uma capacidade específica de descarga inicial de 182 mAh g^{-1} e uma capacidade estabilizada de 179 mAh g^{-1} mesmo após 50 ciclos. Um possível mecanismo de crescimento para a formação dos anéis é discutido.

In this work, a simple one step hydrothermal method to synthesize $\text{Na}_{0.3}\text{V}_2\text{O}_5$ nanofibers/nanorings without using any surfactant at 200 °C in 3-5 days is reported. The products were characterized by X-ray diffractometry (XRD), Fourier transform infrared spectroscopy (FTIR), UV-Vis spectroscopy, scanning electron microscopy (SEM), transmission electron microscopy (TEM) and electrochemical discharge-charge test for lithium ion batteries. XRD patterns showed that, at 200 °C for 2 and 3-4 days, $\text{Na}_{0.3}\text{V}_2\text{O}_5 \cdot 1.5\text{H}_2\text{O}$ belts and $\text{Na}_{0.3}\text{V}_2\text{O}_5$ nanofibers/rings were formed, respectively. The FTIR spectrum revealed peaks at 1003 and 956 cm^{-1} assigned respectively to $\text{V}^{5+}=\text{O}$ and $\text{V}^{4+}=\text{O}$. The UV-Vis spectrum showed maximum absorbance at 404 nm (3.07 eV). TEM analyses revealed a large quantity of fibers 70-100 nm thick and 20-90 μm long, and rings with diameters of ca. 20 μm and thickness of 70-150 nm. The nanofibers/rings exhibited an initial discharge specific capacity of 182 mAh g^{-1} and a stabilized capacity of 179 mAh g^{-1} even after 50 cycles. A possible mechanism for ring formation is discussed.

Keywords: $\text{Na}_{0.3}\text{V}_2\text{O}_5$ nanofibers/nanorings, hydrothermal, lithium ion battery, discharge capacity

Introduction

The synthesis of nanodimensional materials with both specific geometry and morphology is a key point in fields such as modern materials, biotechnology, catalysis, electronics and power sources. In particular, 1D nanostructures with defined geometries have attracted much attention because of their importance in both fundamental science and potential applications in nanodevices.¹ Recently,

it has been demonstrated that several new geometrical configurations such as nanosprings,^{2,3} nanorings,^{2,4-8} and nanohelices^{9,10} grown from 1D nanobelts or nanowires are of special interest owing to their unique periodic and elastic properties that result in structural flexibility and provide additional opportunities for nanoengineering. The ability to construct artificial ring-like building units has implications in the rational design of complex nanostructures for precise nanofabrication. Although much progress has been made in the synthesis of nanorings by coiling of nanobelts, all these successes are based on materials with polar surfaces.^{2,4,9,10}

*e-mail: nagarajugn@rediffmail.com

Metal oxide nanostructured materials, for example, can exhibit unique chemical properties due to their limited size and high density of corner or edge surface sites.¹¹ These properties make nanostructured metal oxides useful for a wide range of applications.^{12,13} In recent years, vanadium oxide compounds, VO_x (such as V_2O_5 , V_2O_4 , V_2O_3 , VO_2 , V_6O_{13}), have been a subject of intensive study. The unique properties of these compounds allow a wide range of practical applications such as electrodes for lithium ion batteries (LIB), electrochromic devices, sensors, transistors, actuators, catalysts and so on.^{7,14-16} Vanadium pentoxide (V_2O_5) is a typical intercalation compound with a layered crystal structure. V_2O_5 has been extensively used as an electrode material for rechargeable LIB because of its low cost, abundance, easy synthesis and high energy density.¹⁷ The theoretical capacity of V_2O_5 with two lithium insertions/extractions (294 mAh g^{-1}) is much higher than those of more commonly used cathode materials, such as LiCoO_2 (145 mAh g^{-1}), LiMn_2O_4 (150 mAh g^{-1}), LiFePO_4 (170 mAh g^{-1}), etc., making it a promising cathode material useful for high power batteries.¹⁵ Moreover, the electrode performance of pure V_2O_5 is enhanced by the addition of alkaline or alkaline-earth metal ions (Li, Na, Mg) into the V_2O_5 host.¹⁸⁻²⁰ These additional alkaline ions are arranged to form pillars between the vanadium oxide layers and thus stabilize the structure during the lithium insertion/extraction. In addition, these pillars increase not only the interlayer space but also the ion diffusion rate.²¹ The structural anisotropy of the particles is believed to induce a better electrochemical response, compared to the analogous compound synthesized by solid state reactions.²² When sufficient sodium is introduced into the van der Waals planes of V_2O_5 , it organizes into a regular and periodic pattern to form sodium-vanadium bronze phases. The most relevant is the β -phase, in which exactly half of the hexagonal interstitial sites are occupied by sodium atoms.²³

Nanostructured materials can provide a high specific surface area and a short ion diffusion pathway compared to that of the bulk, which benefits battery performance.²⁴ Among various methods available to prepare 1D nanostructured $\text{Na}_{0.3}\text{V}_2\text{O}_5$, the solution-based methods are well-known for their advantages in tailoring the size and morphology of the nanostructures.^{22,25-27} Amongst these, the hydrothermal method has several advantages: the control of parameters such as reaction temperature, pH, solvent concentration, as well as the addition of templates or additives, making it possible to obtain samples with different morphologies and structures in a simple manner. Recent literature survey shows that this method is very useful to synthesize doped and also mixed phases with tunable ratios of components.²⁸⁻³¹ To the best of our knowledge,

only few reports are available on the hydrothermal synthesis^{32,33} and electrochemical performance of $\text{Na}_{0.3}\text{V}_2\text{O}_5$ nanorods/particles, especially as a cathode material for rechargeable LIB.^{27,34,35} Hadjean *et al.*³⁴ synthesized $\text{Na}_{0.3}\text{V}_2\text{O}_5$ nanoparticles by the decomposition of aqueous V_2O_5 solution in presence of sodium salt followed by calcination at 500°C . It showed an initial discharge capacity of 230 mAh g^{-1} and reached 195 mAh g^{-1} after 20 cycles. Liu *et al.*³⁵ synthesized $\text{NaV}_6\text{O}_{15}$ nanorods by a hydrothermal method at 205°C for 4 days, followed by calcination at 500°C . It showed an initial discharge capacity of 160 mAh g^{-1} that increased continuously and did not show constant discharge potential. Millet *et al.*²⁷ prepared $\text{Na}_{0.3}\text{V}_2\text{O}_5$ nanoparticles by refluxing at 90°C for 3-4 days followed by calcination at 500°C , showing an initial discharge capacity of 163 mAh g^{-1} that decreased to 50 mAh g^{-1} after 15 cycles. In all the above mentioned cases, the calcination was necessary to get good crystallinity. Higher crystallinity implies better stability of the electrode materials.³⁵

In this article, we report a cost-effective, template-free and low temperature hydrothermal method to synthesize ultrafine nanofibers/rings in acidic medium. The electrode fabricated by the as-synthesized $\text{Na}_{0.3}\text{V}_2\text{O}_5$ nanofibers/rings shows good discharge capacity as well as cycle stability. The synthesized 1D nanofibers/rings structures can efficiently transport charge carriers while maintaining a large surface-to-volume ratio that enhances contact with the electrolyte. The possible growth mechanism for the formation of $\text{Na}_{0.3}\text{V}_2\text{O}_5$ rings is also discussed.

Experimental

Synthesis

270 mg of NaVO_3 were dispersed in 20 mL distilled water taken in a 30 mL capacity Teflon tube. 2-3 drops of HCl (pH ca. 3) were added to the dispersion and stirred for 5 min. The resultant wine-red solution was subjected to hydrothermal treatment at 200°C for 1-5 days. After the hydrothermal treatment, the autoclaves were cooled to room temperature naturally. The reddish-brown non-adherent sponge-like bulky material was centrifuged, washed with distilled water and absolute alcohol before being dried in an oven.

Characterization

Powder X-ray diffraction data were recorded on a Philips X'pert PRO X-ray diffractometer with graphite monochromatized Cu K_α (1.5418 \AA) radiation. The Fourier transform infrared spectrum of the sample was collected on

a Bruker Alpha-P spectrometer. The absorption spectrum of the sample was measured on a Perkin Elmer Lambda-750 UV-Vis spectrometer. The morphology of the product was examined with a JEOL-JSM-6490 LV scanning electron microscope (SEM) and a CM12 Philips transmission electron microscope (TEM).

Electrochemical properties of the $\text{Na}_{0.3}\text{V}_2\text{O}_5$ nanofibers/rings were tested in Swagelok cells assembled in an argon-filled glove box (Jacomex). The electrodes were prepared by mixing $\text{Na}_{0.3}\text{V}_2\text{O}_5$ nanofibers/rings, acetylene black and PVDF (polyvinylidene difluoride) in 70:20:10 ratio. The slurry prepared using NMP (*N*-methylpyrrolidone) as a solvent was coated on aluminium foil as a current collector and finally dried in an oven at about 120 °C for 1 day. Lithium disc was used as counter and reference electrodes. The electrolyte was 1 mol L⁻¹ LiPF₆ in ethylene carbonate and dimethylene carbonate (1:1 v/v). Cyclic voltammetry (CV) measurements were performed using CHI 660C (CH Instruments electrochemical workstation) between 1.5-4.0 V vs. Li⁺/Li at a scan rate of 0.5 mV s⁻¹. Galvanostatic discharge-charge measurements were performed on an Arbin BT-2000 battery tested between 1.5-4.0 V vs. Li⁺/Li at a current density of 0.1 mA g⁻¹.

Results and Discussion

The powder XRD patterns of the samples prepared at 200 °C for 2-4 days are shown in Figure 1. The sample prepared at 200 °C for 2 days (Figure 1, curve a) can be indexed as $\text{Na}_{0.3}\text{V}_2\text{O}_5 \cdot 1.5\text{H}_2\text{O}$.²² It shows a 00l peak series in which the (002) harmonic is missing, suggesting that the double layer structure of the vanadium oxide network is preserved. The basal distance (*d*) of 10.8 Å is consistent with the intercalation of one water layer between the oxide sheets. As the duration of the hydrothermal treatment is increased, the sample is converted to $\text{Na}_{0.3}\text{V}_2\text{O}_5$ (JCPDS No. 21-1175). The hydrated phase of this alkali metal vanadium oxide is characterized by an interlayer spacing of 11 Å.³³ The decrease in the basal distance to *d* = 7.8 Å (at $2\theta = 11.58^\circ$), Figures 1b and 1d, clearly indicates the absence of water between the oxide sheets in the crystal.

In the FTIR spectrum of nanofibers/rings of $\text{Na}_{0.3}\text{V}_2\text{O}_5$ (Figure 2), the vanadium-oxygen stretching vibrations appear in the range of 400-1100 cm⁻¹. The frequencies of the V⁵⁺=O and V⁴⁺=O absorption maxima are 1003 and 956 cm⁻¹, respectively. The bands at 457, 715 and 825 cm⁻¹ correspond to the V-O-V symmetric stretch, V-O-V asymmetric stretch and V-O-V deformation modes, respectively. The bands at 3584 and 1632 cm⁻¹ are due to the symmetric and bending vibration modes of adsorbed water molecule on the surface, respectively.^{36,37}

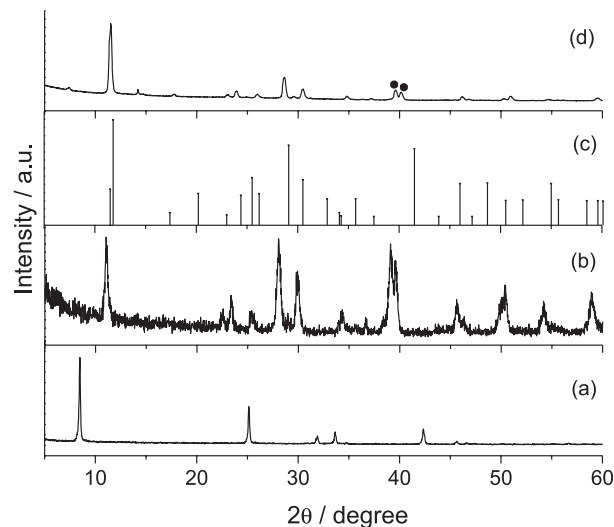


Figure 1. XRD patterns of the (a) $\text{Na}_{0.3}\text{V}_2\text{O}_5 \cdot 1.5\text{H}_2\text{O}$ microbelts at 200 °C for 2 days, (b) $\text{Na}_{0.3}\text{V}_2\text{O}_5$ nanofibers at 200 °C for 3 days, (c) standard XRD pattern of $\text{Na}_{0.3}\text{V}_2\text{O}_5$, JCPDS file No. 21-1175 and (d) $\text{Na}_{0.3}\text{V}_2\text{O}_5$ nanofibers/nanorings at 200 °C for 4 days. (•: $\text{NaV}_3\text{O}_8 \cdot 1.5\text{H}_2\text{O}$).

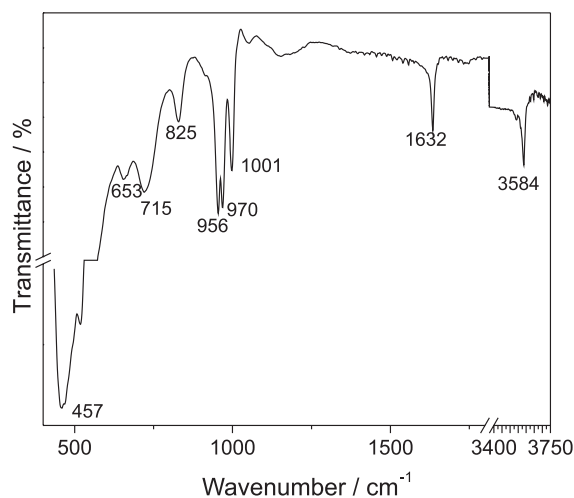


Figure 2. FTIR spectrum of $\text{Na}_{0.3}\text{V}_2\text{O}_5$ nanofibers/nanorings prepared at 200 °C for 4 days.

To evaluate the optical properties of the as-obtained $\text{Na}_{0.3}\text{V}_2\text{O}_5$ nanofibers/rings, the UV-Vis spectrum was recorded from 200 to 800 nm and is shown in Figure 3. The $\text{Na}_{0.3}\text{V}_2\text{O}_5$ nanofibers/rings show maximum absorbance at 404 nm corresponding to a band gap of 3.07 eV. This band corresponds to the $n \rightarrow \pi^*$ transition centered on the V=O group.

Figure 4 shows the SEM images of $\text{Na}_{0.3}\text{V}_2\text{O}_5 \cdot 1.5\text{H}_2\text{O}$ belts prepared at 200 °C for 1-2 days. The belts are 0.5-1.5 μm in width and several tens of micrometers in length. After 2 days, the bending of belts and their increase in length to several micrometers are clearly observed. With further increase in the hydrothermal treatment duration, nanofibers/nanorings are observed. Figure 5 shows the

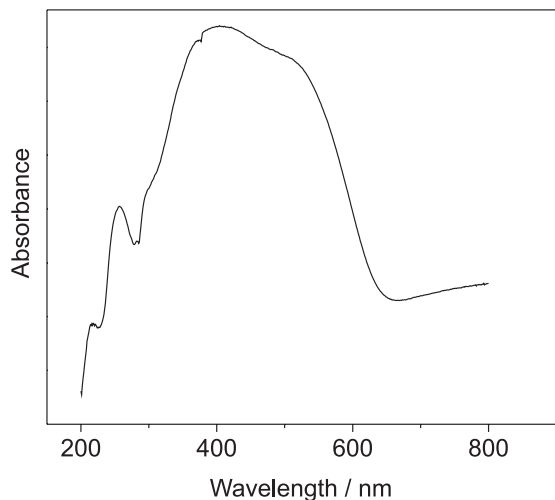


Figure 3. UV-Vis spectrum of $\text{Na}_{0.3}\text{V}_2\text{O}_5$ nanofibers/nanorings prepared at 200 °C for 4 days.

SEM images of $\text{Na}_{0.3}\text{V}_2\text{O}_5$ ultra-fine nanofibers/rings/rods prepared at 200 °C for 3-5 days. The SEM images of the sample prepared at 200 °C for 3 days (Figure 5a) reveal the products having large quantity of the fiber structure with lengths in the range of several tens to hundreds of micrometers. It has been observed that these fibers are flexible. On further increasing the hydrothermal treatment duration to 4 days (Figures 5c and 5d), the formation of concentric nanorings composed of ultrafine nanofibers is clearly observed. The thickness of these nanofibers is 150-600 nm and the length is in the order of several tens of micrometers. The thickness of the rings is about 400 nm and the width is about 10 μm . This shows that bending of the nanofibers leads to the formation of nanorings. On further increasing the hydrothermal treatment time to 5 days (Figures 5d and 5e), morphological changes, i.e., ultrafine fibers to nanorods are noted. The thickness of the nanorods is about 150-500 nm and they are several tens of micrometers in length. But interestingly, the presence of different kinds of rings is observed again. In Figure 5e, the ring is made up of microrods of thickness of about 1.2 μm . The inset of Figure 5e shows that the surface of the rings as well as the microrods are not smooth; instead, they look like humps/twisted threads. Very interestingly, the formed ring

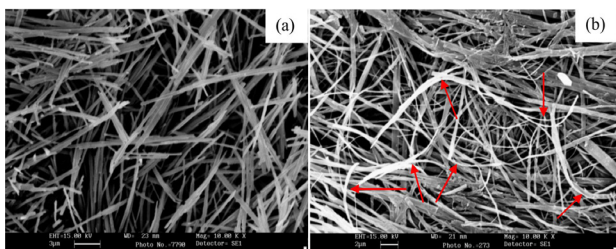


Figure 4. SEM images of $\text{Na}_{0.3}\text{V}_2\text{O}_5 \cdot 1.5\text{H}_2\text{O}$ microrods/belts prepared at 200 °C for (a) 1 day and (b) 2 days.

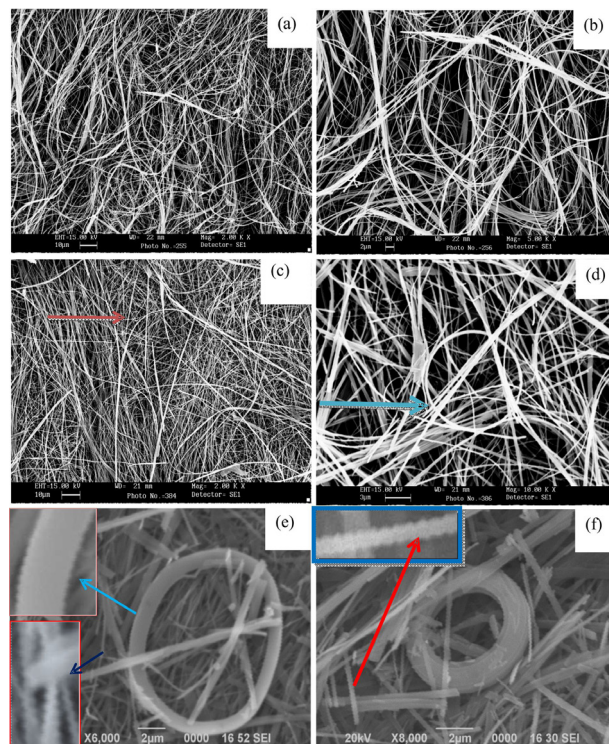


Figure 5. SEM images of $\text{Na}_{0.3}\text{V}_2\text{O}_5$ nanofibers/nanorings prepared at 200 °C for (a and b) 3 days, (c and d) 4 days and (e and f) 5 days.

is an exact look-alike of an automobile tire with an inner diameter of about 3 μm (Figure 5f). The morphology of the nanofibers/rings was further investigated by TEM. Figure 6 shows the TEM image of $\text{Na}_{0.3}\text{V}_2\text{O}_5$ ultra-fine nanofibers/rings prepared at 200 °C for 4 days. It is clearly shown that the thickness of the fiber is uniform along its entire length of about 70-100 nm. The ring shows a thickness of about 70-150 nm.

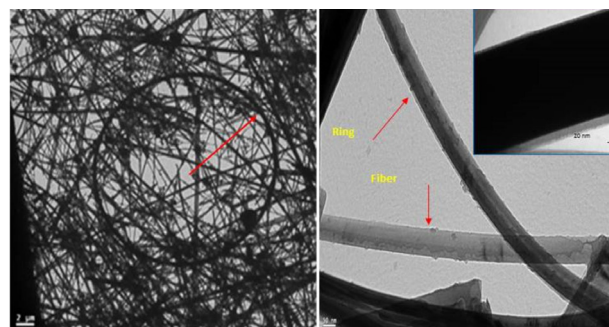


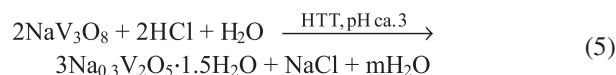
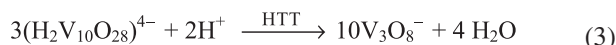
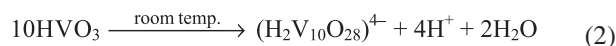
Figure 6. TEM images of $\text{Na}_{0.3}\text{V}_2\text{O}_5$ nanofibers/nanorings prepared at 200 °C for 4 days.

Formation of $\text{Na}_{0.3}\text{V}_2\text{O}_5$ nanorings

It is well-known that the acidification of metavanadate solutions can be conveniently performed via an ion exchange between Na^+ and H^+ in a resin, leading to the formation of $\text{V}_2\text{O}_5 \cdot n\text{H}_2\text{O}$. Na^+ ions are not removed

when acidification is performed by adding an acid; they remain intercalated within the layered oxide leading to poorly crystallized Na_{0.3}V₂O₅·nH₂O. Moreover, the presence of foreign cations introduces new electrostatic interactions leading to flocculation rather than gelation. Two phases can actually be formed upon acidification of sodium metavanadate aqueous solutions, namely, Na_{0.3}V₂O₅·nH₂O and NaV₃O₈·nH₂O. The quantities of the aforesaid compounds depend on experimental conditions, pH, temperature, etc. The hydrated trivanadate is formed above pH 5, while Na_{0.3}V₂O₅·nH₂O is observed below pH 3.5.^{16,22,38,39}

In this process, sodium metavanadate undergoes ionization in aqueous solution, producing Na⁺ and VO₃⁻. The acidification of VO₃⁻ with H⁺ leads to the formation of a wine-red solution of vanadic acid (HVO₃, pH ca. 2), as shown in equation 1. Vanadic acid is then progressively converted into decavanadate ion (H₂V₁₀O₂₈)⁴⁻ (equation 2) and the resulting solution is subjected to the hydrothermal treatment. At the early stage of this treatment, it is expected the decavanadate (H₂V₁₀O₂₈)⁴⁻ species to be protonated and trivanadate to be formed. At low pH, trivanadate is unstable, and finally hydrated sodium vanadate is formed.



Mechanism of ring formation

Several theories/concepts have been put forward to explain the formation of ring structures in the wet chemistry method. Murrey *et al.*⁴⁰ explained the formation of PbSe nanorings by considering the orientation of the dipole moment in PbSe nanocrystals and also the oriented attachment of different faces. The formation of ZnO nanorings by vapor deposition was explained by Wang and co-workers^{41,42} on the basis of the polarity of the molecule. The spontaneous polarization of positively charged Zn²⁺ (0001) and negatively charged O²⁻ (000-1) along the *c*-axis leads to the formation of nanorings. The self-assembly of nanoparticles for the formation of different types of CdS nanorings by the hydrothermal method is explained by Liu and Zeng.⁴³ The formation of single crystalline rutile structure SnO₂ springs, rings and spirals

has been explained based on the the polar charge interaction model.³ The formation of CuO nanorings prepared by hydrothermal methods using sodium dodecyl benzene sulfonate as surfactant was explained by the formation of nanoribbons with polar surfaces that coil into nanorings to reduce the electrostatic energy.⁸ The mechanism of self-coiling of a single nanobelt has been suggested to explain the formation of ZnO nanorings.² Flexible ZnO nanobelts, due to their polar surface, roll into nanorings to reduce the electrostatic energy. The present material, Na_{0.3}V₂O₅ nanofibers/rings synthesized from the solution process in absence of surfactant, has morphologies similar to those of Ag₂V₄O₁₁ nanorings obtained from the hydrothermal method. A similar mechanism may hold well also for the current material.⁴ The structure of Na_{0.3}V₂O₅ can be described as an assembly of stacked V₂O₅ bilayers.

The vanadium coordination is based on VO₅ square pyramids with a short V=O double bond along the *z*-axis perpendicular to the basal planes. Na is intercalated between the vanadium oxide layers. The vanadium oxide layers exhibit a polar structure and positively charged Na⁺ ions can be attracted by the V₂O₅ dipoles on both sides of the bilayers. Moreover, the Na⁺ ions present inside the tunnels along the *b*-axis, in four interstitial equivalent sites *per* unit cell, make the vanadium oxide bilayers favor the flexibility of Na_{0.3}V₂O₅ nanobelts. According to the so-called cation-induced coiling model, when the residual amount of Na⁺ ions from the solution adsorbs asymmetrically at the top or at the bottom of a thin flexible Na nanobelt, asymmetric strain energy is induced. When this induced asymmetric strain energy becomes larger than the elasticity energy, the flexible Na_{0.3}V₂O₅ nanobelt tends to self-coil into a ring. A tentative schematic diagram for the formation of nanorings is shown in Figure 7.

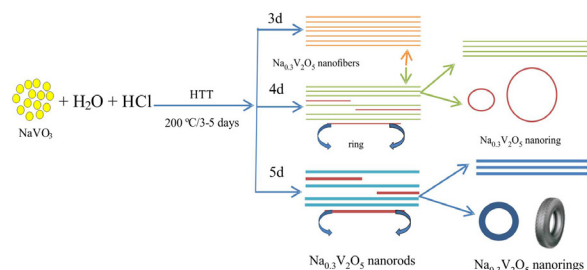


Figure 7. Possible schematic growth diagram of Na_{0.3}V₂O₅ nanofibers/nanorings. HTT = hydrothermal treatment.

Electrochemical performance Na_{0.3}V₂O₅ nanofibers/rings

Figure 8 shows the cyclic voltamogram for the Na_{0.3}V₂O₅ nanofibers/rings prepared at 200 °C for 4 days for lithiation-delithiation in the voltage range of 1.5-4 V vs. Li/Li⁺.

It shows one broad cathodic peak (lithiation) at about 3.5 V and anodic peak (delithiation) at about 2.15 V. In the fourth cycle, the CV curve is nearly intact, except that the anodic peak (1st cycle) at 2.45 V is shifted to 2.15 V. The insertion/extraction behavior of lithium ions thus can be tentatively expressed as:

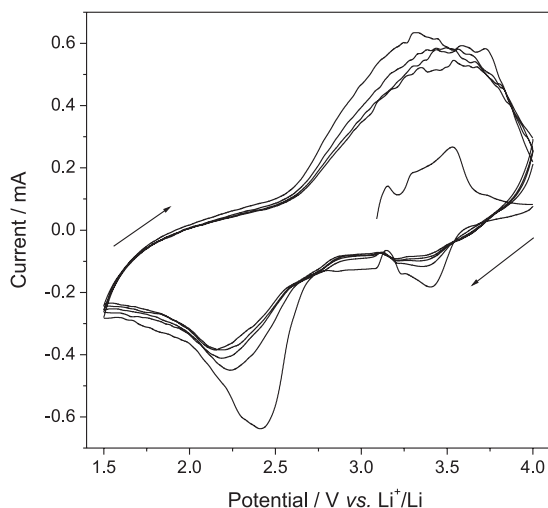


Figure 8. Cyclic voltammogram of $\text{Na}_{0.3}\text{V}_2\text{O}_5$ nanofibers/nanorings prepared at 200 °C for 4 days.

The electrochemical properties of $\text{Na}_{0.3}\text{V}_2\text{O}_5$ nanofibers/rings as cathodes in lithium ion storage were tested via charge-discharge measurement at a current density of 0.1 mA g⁻¹ as shown in Figure 9. The specific capacity of $\text{Na}_{0.3}\text{V}_2\text{O}_5$ nanofibers/rings increased in the beginning from 181 mAh g⁻¹, reached a maximum capacity of 200 mAh g⁻¹, became relatively stable in the further cycles and finally reached a capacity of 179 mA h g⁻¹ after the fiftieth cycle. At the same time, it was also noticed that the capacity increased from the first to the third cycle, and then gradually stabilized during the subsequent discharge-charge cycles. In fact, this capacity increase in the initial stage is not an accidental result. It was reported that some materials prepared by low temperature methods exhibited amorphous nature and nanocrystalline phase. The increased capacity is most probably due to the relaxation of the amorphous structure to create a smooth pathway for the lithium ion insertion and extraction during the initial stage of the cell operation.⁴⁴ The $\text{Na}_{0.3}\text{V}_2\text{O}_5$ monoclinic structure remains stable all along the Li insertion process, which makes this compound very attractive as rechargeable cathodic material for lithium cells.²⁶ Figure 10 shows that the discharge profile exhibits one plateau, which is consistent with the cyclic voltammogram. The average coulombic efficiency at different currents is no less than 85% from the first cycle

to the 50th, and the enhanced Li insertion properties are relevant to the increased crystallinity of the material. These results indicate that the $\text{Na}_{0.3}\text{V}_2\text{O}_5$ nanofibers/nanorings synthesized by this hydrothermal method are promising cathode materials in lithium-ion batteries.

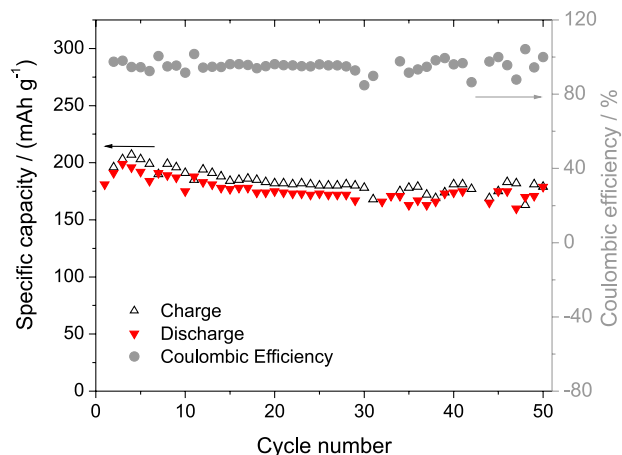


Figure 9. Specific capacity vs. cycle number and Coulombic efficiency of $\text{Na}_{0.3}\text{V}_2\text{O}_5$ nanofibers/nanorings prepared at 200 °C for 4 days.

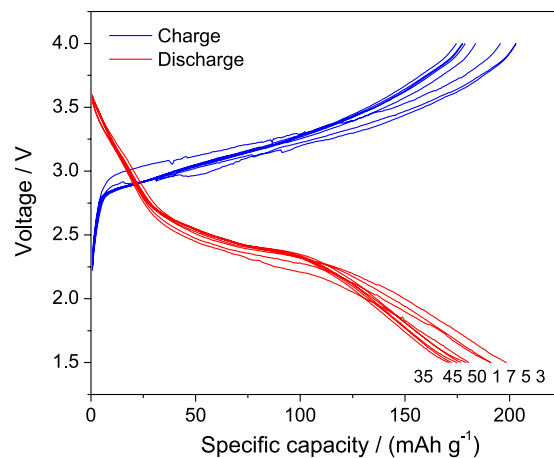


Figure 10. Discharge-charge profile of $\text{Na}_{0.3}\text{V}_2\text{O}_5$ nanofibers/nanorings prepared at 200 °C for 4 days.

Conclusion

In this work, a facile one step hydrothermal route to synthesize $\text{Na}_{0.3}\text{V}_2\text{O}_5 \cdot n\text{H}_2\text{O}$ microrods/nanofibers/nanorings without using any surfactant in acidic medium (pH ca. 3) was demonstrated. Following the increase in the hydrothermal treatment time from 2 to 3 days at 200 °C, the layered structure of $\text{Na}_{0.3}\text{V}_2\text{O}_5 \cdot 1.5\text{H}_2\text{O}$ changes to the tunnel structure of $\text{Na}_{0.3}\text{V}_2\text{O}_5$. The resulting $\text{Na}_{0.3}\text{V}_2\text{O}_5$ nanofibers are 70-100 nm in thickness and several tens of micrometers in length. The ring shows a concentric diameter of about 20 μm and thickness of about 70-150 nm. The rings are predominantly formed due to the self-coiling

of polar surface Na_{0.3}V₂O₅ nanofibers. Electrochemical tests show that the Na_{0.3}V₂O₅ nanofibers/rings have an initial specific capacity of 181 mAh g⁻¹ in the potential range of 1.5–4 V and that its stabilized capacity still remained as high as 179 mA hg⁻¹ after 50 cycles. Compared to V₂O₅, the structural changes by Li insertion into β-Na_{0.3}V₂O₅ are stable. The resulting Na_{0.3}V₂O₅ nanofibers/nanorings are a promising cathode material for lithium-ion batteries.

Acknowledgements

Dr. Nagaraju thanks Dr. G. T. Chandrappa (Department of Chemistry, Bangalore University, Bangalore) for the discussion on vanadium chemistry, Prof. S. Sampath (Department of Inorganic and Physical Chemistry, Indian Institute of Science, Bangalore) for providing electrochemical measurements and Prof. Jairton Dupont (Department of Molecular Catalysis, UFRGS, Porto Alegre, Brazil) for providing the TEM facility.

References

- Mohan, V. M.; Hu, B.; Qiu, W.; Chen, W.; *J. Appl. Electrochem.* **2009**, *39*, 2001.
- Kong, X. Y.; Ding, Y.; Yang, R. S.; Wang, Z. L.; *Science* **2004**, *303*, 1348.
- Yang, R.; Wang, Z. L.; *J. Am. Chem. Soc.* **2006**, *128*, 1466.
- Shen, G. Z.; Chen, D.; *J. Am. Chem. Soc.* **2006**, *128*, 11762.
- Ashoka, S.; Nagaraju, G.; Chandrappa, G. T.; *Mater. Res. Bull.* **2010**, *45*, 1736.
- Chandrappa, G. T.; Chithaiah, P.; Ashoka, S.; Livage, J.; *Inorg. Chem.* **2011**, *50*, 7421.
- Liu, J.; Xue, D.; *Nanoscale Res. Lett.* **2010**, *5*, 1619.
- Wang, X.; Xi, G.; Xiong, S.; Liu, Y.; Xi, B.; Yu, W.; Qian, Y.; *Cryst. Growth Des.* **2007**, *7*, 930.
- Yu, D.; Wu, J. Q.; Gu, Q.; Park, H. K.; *J. Am. Chem. Soc.* **2006**, *128*, 8148.
- Nath, M.; Parkinson, B. A.; *J. Am. Chem. Soc.* **2007**, *129*, 11302.
- García, M. F.; Arias, A. M.; Hanson, J. C.; Rodriguez, J. A.; *Chem. Rev.* **2004**, *104*, 4063.
- Pinna, N.; Neri, G.; Antonietti, M.; Niederberger, M.; *Angew. Chem., Int. Ed.* **2004**, *43*, 4345.
- Viswanatha, R.; Sapra, S.; Gupta, S. S.; Satpati, B.; Satyam, P. V.; Dev, B. N.; Sarma, D. D.; *J. Phys. Chem. B* **2004**, *108*, 6302.
- Pan, A.; Zhang, J. G.; Nie, Z.; Cao, G.; Arey, B. W.; Li, G.; Liang, S. Q.; Liu, J.; *J. Mater. Chem.* **2010**, *20*, 9193.
- Wang, S.; Lu, Z.; Wang, D.; Li, C.; Chen, C.; Yin, Y.; *J. Mater. Chem.* **2011**, *21*, 6365.
- Livage, J.; *Coord. Chem. Rev.* **1999**, *391*, 190.
- Yu, D.; Chen, C.; Xie, S.; Liu, Y.; Park, K.; Zhou, X.; Zhang, Q.; Li, J.; Cao, G.; *Energy Environ. Sci.* **2011**, *4*, 858.
- Pistoia, G.; Pasquali, M.; Wang, G.; Li, L.; *J. Electrochem. Soc.* **1990**, *137*, 2365.
- Maingot, S.; Baffier, N.; Ramos, J. P.; Willman, P. A.; *Solid State Ionics* **1993**, *67*, 29.
- Manev, V.; Momchilov, A.; Nassalevska, A.; Pistoia, G.; Pasquali, M.; *J. Power Sources* **1995**, *54*, 501.
- Spahr, M. E.; Novak, P.; Scheifele, W.; Haas, O.; Nesper, R.; *J. Electrochem. Soc.* **1998**, *145*, 421.
- Durupthy, O.; Steunou, N.; Coradin, T.; Maquet, J.; Bonhomme, C.; Livage, J.; *J. Mater. Chem.* **2005**, *15*, 1090.
- Darling, R. B.; Iwanaga, S.; *Sadhana* **2009**, *34*, 531.
- Lou, X. W.; Deng, D.; Lee, J. Y.; Feng, J.; Archer, L. A.; *Adv. Mater.* **2008**, *20*, 258.
- Pereira-Ramos, J. P.; Messina, R.; Znaidi, L.; Baffier, R.; *Solid State Ionics* **1986**, *28-30*, 886.
- Pereira-Ramos, J. P.; Baddour, R.; *Solid State Ionics* **1992**, *53-56*, 701.
- Millet, M.; Farcy, J.; Pereira-Ramos, J. P.; Sabbar, E. M.; De Roy, M. E.; Besse, J. P.; *Solid State Ionics* **1998**, *112*, 319.
- Meng, F.; Li, J.; Hong, Z.; Zhi, M.; Sakla, A.; Xiang, C.; Wu, N.; *Catal. Today* **2013**, *199*, 48.
- Shen, X.; Tian, B.; Zhang, J.; *Catal. Today* **2013**, *201*, 151.
- Shen, X.; Zhang, J.; Tian, B.; Anpo, M.; *J. Mater. Sci.* **2012**, *47*, 5743.
- Meng, F.; Hong, Z.; Arndt, J.; Li, M.; Zhi, M.; Yang, F.; Wu, N.; *Nano Res.* **2012**, *5*, 213.
- Zhou, G. T.; Wang, X.; Yu, J. C.; *Cryst. Growth Des.* **2005**, *5*, 969.
- Yao, T.; Oka, Y.; Yamamoto, N.; *J. Mater. Chem.* **1992**, *2*, 331.
- Hadjean, R. B.; Bach, S.; Emery, N.; Ramos, J. P.; *J. Mater. Chem.* **2011**, *21*, 11296.
- Liu, H.; Wang, Y.; Li, L.; Wang, K.; Hosono, E.; Zhou, H.; *J. Mater. Chem.* **2009**, *19*, 7885.
- Volkov, V. L.; Zakharova, G. S.; Podvalnaya, N. V.; Kuznetsov, M. V.; *Russ. J. Inorg. Chem.* **2008**, *53*, 854.
- Fei, H. L.; Liu, M.; Zhou, H. J.; Sun, P. C.; Ding, D. T.; Chen, T. H.; *Solid State Sci.* **2009**, *11*, 102.
- Livage, J.; *Chem. Mater.* **1991**, *3*, 578.
- Livage, J.; *Materials* **2010**, *3*, 4175.
- Cho, K. S.; Talapin, D. V.; Gaschler, W.; Murray, C. B.; *J. Am. Chem. Soc.* **2005**, *127*, 7140.
- Li, F.; Ding, Y.; Gao, P. X.; Xin, X. Q.; Wang, Z. L.; *Angew. Chem., Int. Ed.* **2004**, *43*, 5238.
- Peng, Y.; Xu, A. W.; Deng, B.; Antonietti, M.; Colfen, H.; *J. Phys. Chem. B* **2006**, *110*, 2988.
- Liu, B.; Zeng, H. C.; *J. Am. Chem. Soc.* **2005**, *127*, 18262.
- Liu, H.; Wang, Y.; Wang, K.; Hosono, E.; Zhou, H.; *J. Mater. Chem.* **2009**, *19*, 2835.

Submitted: January 25, 2013

Published online: September 4, 2013